

Title: Evaluation and Prediction of the Tensile Properties of Continuous Fiber-Reinforced 3D Printed Structures

Authors: Garrett W. Melenka^a, Benjamin K.O. Cheung^a, Jonathon S. Schofield^a, Michael R. Dawson^b, Jason P. Carey^{a*}

^a*Mechanical Engineering, Faculty of Engineering, University of Alberta, Edmonton Alberta T6G 1H9, Canada*

^b*Glenrose Rehabilitation Hospital, Edmonton, Alberta, Canada, T6G 2E1*

Corresponding Author: Jason. P.R. Carey, PhD, Peng

Corresponding Author's Institution: University of Alberta

First Author: Garrett W. Melenka, MSc.

Order of Authors: Garrett Melenka, MSc.; Benjamin K Cheung, BSc; Jonathon S Schofield, MSc; Michael R Dawson, MSc; Jason P Carey, PhD

*Corresponding Author E-mail: jpcarey@ualberta.ca

Keywords: 3D Printing; Elastic Properties; Fiber Reinforced 3D Printing; Mechanical Properties; Volume Average Stiffness; 3D Printed Composites

Abstract

Three dimensional (3D) printing is a technique conventionally used to manufacture prototypes. Commercial desktop 3D printers have become available which produce functional 3D printed parts. The MarkOne by Mark Forged manufactures printed structures reinforced with continuous Carbon, Fiberglass or Kevlar fibers. The aim of this study is to evaluate the elastic properties of the fiber reinforced 3D printed structures and predict elastic properties using an Average Stiffness (VAS) method. Samples evaluated in this study were produced by varying the volume fraction of fibers within the 3D printed structures (4.04, 8.08 and 10.1% respectively). The experimentally determined elastic modulus was found to be 1767.2, 6920.0 and 9001.2 MPa for fiber volume fractions of 4.04, 8.08 and 10.1% respectively. The predicted elastic moduli were found to be 4155.7, 7380.0 and 8992.1 MPa. The model results differed from experiments by 57.5, 6.2 and 0.1% for the 4.04, 8.08 and 10.1% fiber volume fractions. The predictive model allows for the elastic properties of fiber reinforced 3D printed parts. The model presented will allow for designers to predict the elastic properties of fiber reinforced 3D printed parts to be used for functional components which require specific mechanical properties.

1 Introduction

Three dimensional (3D) printing or Rapid Prototyping (RP) is a manufacturing process that produces components from computer-aided design (CAD) software. Three dimensional printing is not an entirely new technology but the advent of open source, low cost 3D printers has led to drastic proliferation of this technology. This process has become highly popular with researchers and hobbyists for the design and manufacture of 3D parts as it allows for the rapid design and manufacture of complex component.

3D printing can be divided into several categories: Fused Deposition Modeling (FDM), Selective Laser Melting (SLM), Stereolithography (STL) or Laminated Object Manufacturing (LOM) [1]. Most low-cost desktop 3D printers utilize FDM as the manufacturing process. FDM forms a 3D geometry by assembling individual layers of extruded thermoplastic filament. The FDM manufacturing process is useful for rapidly producing prototypes and in some cases can be used to produce functional components. However, there are disadvantages to utilizing FDM printed parts for functional components. FDM components are formed by an additive manufacturing process combining successive layers of molten thermoplastic. Due to this process delamination of the component layers can occur resulting in premature failure. Additionally, FDM printed parts typically have lower elastic properties than injection molded components of the same thermoplastics [2].

Several authors have evaluated the mechanical properties of FDM 3D printed parts [3, 4]. The primary focus of these studies has been on conventional FDM printed components [3-5]. These studies have evaluated both commercial FDM 3D printers [3-5] as well as low-cost desktop 3D printers [2]. Currently, new thermoplastic materials are becoming available; these include thermoplastic filaments with embedded metallic particles or reinforced with short carbon fibers [6, 7]. Additionally, a new 3D printer has become commercially available that reinforces 3D printed parts with continuous Glass Fiber, Kevlar Fiber or Carbon Fiber filaments (the MarkOne by MarkForged). This new 3D printer, MarkOne by MarkForged, is designed to produce functional 3D printed parts which are stronger than conventional FDM printed components. The MarkOne 3D printer reinforces FDM printed parts by embedding concentric rings of fibers that follow the components geometry. Specifically, the objective of these new FDM printing methods

is to increase the strength of 3D printed parts so that these components can be used for functional products rather than producing non-functional scale models. Currently, continuous fiber reinforced 3D printed parts have not been extensively investigated in literature. The use of continuous carbon fiber reinforcement was performed by Mori *et al* using a RepRap based 3D printer; however, this study did not evaluate or determine the elastic properties of the carbon fiber reinforced 3D printed components [8]. Understanding the tensile properties of fiber reinforced 3D printed components is necessary to ensure these components meet their required design specifications.

To determine if continuous fiber reinforced FDM printed components can be used for functional components, the mechanical properties need to be determined. As a fundamental first step, the first objective of this study is to evaluate the tensile properties of continuous fiber reinforced 3D printed components produced using the MarkOne 3D printer by performing conventional tensile tests. The second objective of this study is to develop a methodology that allows designers to predict the elastic constants of continuous fiber FDM printed components. Conventional composite material modeling techniques, such as classical laminate plate theory (CLPT) or volume averaging methods [3, 5, 9-12], can be applied to these materials in order to predict its mechanical properties.

Based on the aforementioned composite material modeling framework a mathematical model for predicting the tensile elastic properties of fiber reinforced 3D printed components will be presented. The results of this study aims to provide designers with a methodology for determining the mechanical properties of fiber reinforced 3D printed components. The presented mathematical model will reduce the need for multiple design iterations in order to produce functional 3D printed components.

2 Methods

2.1 Mechanical Testing

Samples for mechanical testing were fabricated using a MarkOne desktop 3D printer (MarkOne, MarkForged, Somerville, MA). The sample geometry was created according to ASTM D638-14 (ASTM D638-14 Standard Test Method for Tensile Properties of Plastics) using a Type I geometry [13]. The geometry used in this study and critical dimensions are shown in Figure 1. The test specimen geometry was created using a computer aided design (CAD)

software package (SolidWorks 2015 SP4.0, Dassault Systems, Waltham, MA). The specimen geometry was exported as a stereolithography file (STL) and loaded into a 3D printer slicing software package (Eiger 1.2, MarkForged, Somerville, MA). The Eiger software package is required to control the placement of the fiber reinforcement, therefore other open-source 3D printing software was not used. All samples were printed with a nylon filament (Nylon, MarkForged, Somerville, MA) with Kevlar fiber reinforcement (Kevlar Reinforcement, MarkForged, Somerville, MA).

The printing parameters used to manufacture the test specimen are summarized in Table 1. The MarkOne 3D printer reinforces printed structures using continuous Kevlar, Carbon or Glass fibers. For this study, Kevlar fibers were utilized to reinforce the test specimens. Kevlar was chosen due to the research group's prior experience with this material [14-17]. Three dimensional printed samples are reinforced with concentric fiber rings. The number of possible rings ranges from none (pure polymer) to 5 rings for this geometry; with the limiting factor being the thin 13mm (WN) neck region. The number of concentric fiber rings was varied to quantify the effect of concentric rings on the mechanical properties of the 3D printed test specimen. Samples were printed with 5, 4, 2 and no concentric fiber rings. The number of concentric rings used in this study was selected to characterize the effect of fiber reinforcement on 3D printed samples over the spectrum of possible fiber reinforcement values. The reinforcement of the test specimens with Kevlar yarns is shown in Figure 2.

Table 1: Test specimen print parameters

Print Parameters	
Layer Height (mm)	0.1
Infill Percentage (%)	10
Infill Orientation (degrees)	45
Number of infill layers	8
Shell Thickness (mm)	0.4
Number of Shells	2
Number of floor layers	4
Number of ceiling layers	4
Number of solid layers	8
Total number of layers	32

2.1.1 Dimensional Measurement of Samples

Prior to performing mechanical tests, Kevlar reinforced 3D printed samples were measured to evaluate the dimensional accuracy of the MarkOne 3D printer. The width at end tabs (W), gauge section width (WN) and thickness (T), shown in Figure 1, were measured; the latter three using a micrometer (0-25 \pm 0.01mm Mitutoyo 102-0701, Kawasaki, Japan). For each test sample dimension (W , WN and T), five measurements were recorded.

2.1.2 Testing Parameters

The fiber reinforced 3D printed specimens were evaluated by performing tensile tests. The test setup used to evaluate the 3D printed samples is shown in Figure 3. An MTS tensile testing frame (MTS 810 Material Test System, MTS, Eden Prairie, USA) with a 100 KN (22 Kip) load cell was used to apply loads to the test specimen. Strain of the test samples was measured using a 25.4 mm (1”) gauge length extensometer (MTS 634.12E-24, MTS, Eden Prairie, USA). Samples were loaded at a rate of 0.5mm/min and data from the load cell and extensometer was collected at a rate of 20Hz.

2.2 Optical Microscopy

Test samples used in this study were examined using an optical microscope. Optical microscopy was performed in order to gain insights into the internal structure of the 3D printed samples and to examine the failure mechanism for these samples. Samples were mounted using cold cure epoxy resin (Cold Cure, System Three Resins, Inc., Auburn, WA, USA) in 1" diameter sample cups (Buehler Canada, Whitby, ON, Canada). Resin and hardener were mixed, according to manufacturer specifications, at a ratio of 2:1 and poured over sample sections of the fiber reinforced 3D printed parts. The resin was allowed to cure at room temperature for a minimum of 12 hours.

Following curing, the samples were then prepared using a 4-step method to ready the samples for imaging. First, samples were ground until plane using a 320 grit SiC paper, and large scratches were removed using a 600 grit SiC paper. The sample was then polished using diamond suspensions on polishing cloths, beginning at 9-micron monocrystalline diamond suspensions followed by a 3-micron monocrystalline diamond suspension. Final polishing was performed with a 0.05-micron alumina suspension on polishing cloth. All consumables were supplied from Buehler Canada. The sample polishing procedure is outlined in Table 2.

Table 2: Outline of sample preparation for imaging

Task	Surface
Grinding	320 grit SiC paper
Grinding	600 grit SiC paper
Polishing	9 micron diamond suspension, polishing cloth
Polishing	3 micron diamond suspension, polishing cloth
Final polishing	0.05 micron alumina suspension, polishing cloth

Samples were then imaged using a high resolution camera (Basler piA2400-17gm, Basler AG, Ahrensburg, DE) mounted with a variable magnification lens (Infiniprobe MS, Infinity USA, Boulder, CO, USA). The magnification of this particular set of images was between 2x and 3x, thus in the final images the pixel width is approximately 1 to 2 μm .

2.3 Prediction of Elastic Constants

A new volume averaging method has been implemented in order to predict the elastic constants of fiber reinforced 3D printed parts. The volume averaging method utilized is an analytical model based on a volume average stiffness method to predict the effective elastic constants of a fiber reinforced 3D printed part [10]. The fiber reinforced 3D printed parts consist of several different regions, each with their own elastic constants. The analytical model allows for the contribution of each of these regions to be accounted for in order to predict the effective elastic modulus of the fiber reinforced 3D printed specimen. The analytical model has been developed as a custom MATLAB script (MATLAB 2015a, The MathWorks, Natick, MA) to allow for rapid computation of the mechanical properties of a 3D printed structure.

In order to predict the mechanical properties of the Kevlar-reinforced 3D printed samples the mechanical properties of the nylon filament and Kevlar reinforcement were assumed as the specific mechanical properties were not specified by the manufacturer. The assumed mechanical properties for the nylon filament and Kevlar fibers are summarized in Table 3 and Table 4 respectively [18, 19].

Table 3: Assumed elastic constants of Nylon filament [19]

Material Property	Value
Elastic Modulus $-E$ (GPa)	0.35- 3.5
Shear Modulus G (GPa)	0.13- 1.30
Poisson's ratio - ν	0.35

Table 4: Assumed elastic constants of Kevlar 29 yarns [18]

Material Property	Value
Longitudinal Elastic Modulus $-E_{f1}$ (GPa)	79.8
Transverse Elastic Modulus E_{f2} (GPa)	2.59
In-plane Shear Modulus G_{f12} (GPa)	2.1
Poisson's ratio $- \nu_{12}$	0.33
Poisson's ratio - ν_{23}	0.1

2.3.1 *Internal Microstructure*

A schematic of the internal structure of the fiber reinforced 3D printed specimen is shown in Figure 4. It can be seen that four distinct regions exist within the test samples: shell layers form the external structure of the test specimen where the extruded nylon is oriented along the longitudinal axis of the test specimen; solid layers which consist of closed layers of nylon and alternate orientation between $\pm 45^\circ$ from the longitudinal axis; infill layers which consist of sparse layers of nylon. Similar to the solid layers, infill layers alternate orientation between $\pm 45^\circ$ from the longitudinal axis; and, Kevlar layers which consist of concentric rings of Kevlar fibers. The Kevlar fibers are oriented along the longitudinal axis of the test sample. The Kevlar layers also consist of infill regions as the Kevlar yarns do not fill the entire cross-section of the test samples.

A cross-sectional image that shows the internal structure of a single test specimen is shown in Figure 5, in which infill and shell regions can be seen. A top view of a test specimen is also shown in Figure 6. Here, the orientation of the solid layers is 45° from the longitudinal axis of the test specimen. The schematic in Figure 4 and the images in Figure 5 and Figure 6 will be used to determine the geometry and structure of the test sample.

The volume fraction of each component of the test specimen was determined from the geometry of the sample. The dimensions of the individual components within the test specimen are summarized in Table 5. The variables summarized in Table 5 were used to calculate the volume (in mm^3) of each component using equations 1-7.

Table 5: Sample geometry internal dimensions

Sample Geometry Variable	Value
Height (H)-mm	57
Width (W)-mm	13
Thickness (T)- mm	3.2
Width of Fiber(W_{fiber}) - mm	0.7
Number of fiber layers (N_{fiber})	6
Number of fiber concentric rings ($N_{\text{concentric}}$)	5,4,2,0
Layer Thickness (T_{layer}) - mm	0.1
Number of Floor Layers (N_{floor})	4
Number of Ceiling Layers (N_{ceiling})	4
Number of Solid Layers (N_{solid})	8

The total sample volume (V_{tensile}) is:

$$V_{\text{tensile}} = H \cdot W \cdot T \quad (1)$$

The floor volume (V_{floor}) is given by:

$$V_{\text{floor}} = [W - (W_{\text{shell}} \cdot 2)] \cdot H \cdot T_{\text{layer}} \cdot N_{\text{floor}} \quad (2)$$

The ceiling volume (V_{ceiling}) is given by:

$$V_{\text{ceiling}} = [W - (W_{\text{shell}} \cdot 2)] \cdot H \cdot T_{\text{layer}} \cdot N_{\text{ceiling}} \quad (3)$$

The solid volume (V_{solid}) is found as:

$$V_{\text{solid}} = [W - (W_{\text{shell}} \cdot 2)] \cdot H \cdot T_{\text{layer}} \cdot N_{\text{solid}} \quad (4)$$

The infill volume (V_{infill}) is given by:

$$V_{infill} = [W - (W_{shell} \cdot 2)] \cdot H \cdot T_{layer} \cdot N_{infill} \quad (5)$$

The fiber volume (V_{kevlar}) is found as:

$$V_{kevlar} = W_{fiber} \cdot T_{layer} \cdot N_{concentric} \cdot 2 \cdot N_{fiber} \quad (6)$$

The infill Volume in Fiber Region ($V_{infillFiber}$) mm^3 is given by:

$$V_{infillfiber} = [W - (2 \cdot W_{shell}) - (W_{fiber} \cdot N_{concentric} \cdot 2)] \cdot T_{layer} \cdot H \cdot N_{fiber} \quad (7)$$

The volume fraction of each section of the test specimen is computed using Equations (8) – (12).

Where the volume fraction of the floor (V_{ffloor}) and ceiling ($V_{fceiling}$) layers are found using:

$$V_{ffloor} = \frac{V_{floor}}{V_{tensile}} \quad (8)$$

$$V_{fceiling} = \frac{V_{ceiling}}{V_{tensile}} \quad (9)$$

The volume fractions of the solid (V_{fsolid}) and infill layers ($V_{finfill}$) are found using:

$$V_{fsolid} = \frac{V_{solid}}{V_{tensile}} \quad (10)$$

$$V_{finfill} = \frac{V_{infill}}{V_{tensile}} \quad (11)$$

And finally, the volume fraction of the Kevlar Fibers ($V_{fkevlar}$) is found using:

$$V_{fkevlar} = \frac{V_{kevlar}}{V_{tensile}} \quad (12)$$

2.3.2 Volume Average Stiffness Method

The effective elastic constants of the fiber reinforced 3D printed samples will be determined using a volume average stiffness method [9-12]. The volume averaging method involves three main steps. First, micromechanical models are used to determine the effective properties of the FDM printed components. Second, a coordinate system transformation is applied to the solid and infill layers. Third, volume averaging of the stiffness matrices of each of the cross-sectional regions is performed.

To determine the micromechanical properties of the solid, infill and shell regions the model developed by Rodriguez *et al.* is used to determine the unidirectional constants for a FDM component [5]. The model of Rodriguez *et al.* treats FDM-printed parts as a plastic/void composite. The elastic properties for Nylon shown in Table 3 were used to determine the micromechanical properties of the shell, infill and solid layers. Equations (13) – (17) are used to determine the mechanical properties of the FDM printed sections. In equations (13) – (17) ρ_1 represents the void density in each component. Void density for the solid layers was assumed to be 10% while the infill sections were assumed to have a void density of 90%. Equations (13) – (17) demonstrate that the FDM printed portions of the test specimen will behave in a transversely isotropic manner.

$$E_{11} = (1 - p_1)E \quad (13)$$

$$E_{22} = (1 - p_1^{1/2})E \quad (14)$$

$$G_{12} = G \frac{(1 - p_1)(1 - p_1^{1/2})}{(1 - p_1) + (1 - p_1^{1/2})} \quad (15)$$

$$\nu_{12} = (1 - p_1)\nu \quad (16)$$

$$\nu_{21} = (1 - p_1^{1/2})\nu \quad (17)$$

Once the micromechanical properties of the solid, infill and shell regions are determined the compliance matrix of each region can be populated. The compliance matrix for a transversely isotropic material is shown in (18).

$$[S] = \begin{bmatrix} \frac{1}{E_1} & -\frac{\nu_{21}}{E_2} & -\frac{\nu_{31}}{E_3} & 0 & 0 & 0 \\ -\frac{\nu_{12}}{E_1} & \frac{1}{E_2} & -\frac{\nu_{32}}{E_3} & 0 & 0 & 0 \\ -\frac{\nu_{13}}{E_1} & -\frac{\nu_{23}}{E_2} & \frac{1}{E_3} & 0 & 0 & 0 \\ 0 & 0 & 0 & \frac{1}{G_{23}} & 0 & 0 \\ 0 & 0 & 0 & 0 & \frac{1}{G_{13}} & 0 \\ 0 & 0 & 0 & 0 & 0 & \frac{1}{G_{12}} \end{bmatrix} \quad (18)$$

The solid and infill regions of the test specimen are transformed using the rotation matrix, $[T]$, shown in equation (19). In this equation c represents cosine and s represents sine and θ is the angle of the solid and infill layers. The new stiffness matrix $[S_{xyz}]$ relative to the global specimen coordinate system is determined for all solid and infill layers.

$$S_{XYZ} = [T]^T [S'_{xyz}] [T] \quad (19)$$

where

$$[T] = \begin{bmatrix} c^2 & s^2 & 0 & 0 & 0 & 2cs \\ s^2 & c^2 & 0 & 0 & 0 & -2cs \\ 0 & 0 & 1 & 0 & 0 & 0 \\ 0 & 0 & 0 & c & s & 0 \\ 0 & 0 & 0 & -s & c & 0 \\ -cs & cs & 0 & 0 & 0 & c^2 - s^2 \end{bmatrix}$$

and

$$c = \cos(\theta)$$

$$s = \sin(\theta)$$

The stiffness averaging is performed by determining the volume fraction of each section within the test specimen in order to determine the contribution of each section to the overall mechanical properties. The stiffness averaging equation used to predict the mechanical

properties of the test specimen is shown in (20). This equation shows that the contribution of the infill, shell, solid and Kevlar fiber regions are taken into account in order to determine the effective properties of the fiber reinforced 3D printed test specimen.

$$\begin{aligned} [C^G] = & V_{fshell} [C_{shell}] + V_{f\text{infill}-\theta} [C_{\text{infill}-\theta}] + V_{f\text{infill}+\theta} [C_{\text{infill}+\theta}] + \\ & V_{fsolid-\theta} [C_{solid-\theta}] + V_{fsolid+\theta} [C_{solid+\theta}] + V_{fkevlar} [C_{kevlar}] \end{aligned} \quad (20)$$

To determine the effective mechanical properties of the fiber reinforced 3D printed parts the global stiffness matrix is inverted as shown in (21). Finally, the effective elastic constants can be determined as shown in equation (22).

$$S^G = [C^G]^{-1} \quad (21)$$

$$\begin{aligned} E_x &= \frac{1}{S^g_{11}}, \quad E_y = \frac{1}{S^g_{22}}, \quad E_z = \frac{1}{S^g_{33}} \\ G_{xy} &= \frac{1}{S^g_{66}}, \quad G_{yz} = \frac{1}{S^g_{44}}, \quad G_{xz} = \frac{1}{S^g_{55}} \\ \nu_{xy} &= \frac{-S^g_{12}}{S^g_{11}}, \quad \nu_{zx} = \frac{-S^g_{13}}{S^g_{33}}, \quad \nu_{yz} = \frac{-S^g_{23}}{S^g_{22}} \end{aligned} \quad (22)$$

3 Results

3.1 Dimensional Measurement

Geometric measurements of the test samples were performed to evaluate the consistency of the MarkOne 3D printer. Measurements were also required in order to determine the cross-sectional area of the test samples. The geometric measurements of the test samples were compared with the nominal dimensions for the ASTM D638 Type I dogbone sample shown in Figure 1. The width of the narrow section (WN), width at both end tabs (W1 and W2) and sample thickness (T) was compared for all samples. A *t*-test was used to compare the nominal

sample dimensions with the measured sample dimensions. A p -value of <0.05 was used as the criteria to indicate that a statistically significant difference exists between the nominal sample and measured sample dimensions. The resulting sample measurements and comparison with the nominal sample dimensions are summarized in Table 6- Table 9**Error! Reference source not found.** From these tables it can be seen that the sample dimensions deviated from the nominal dimensions. A similar measurement method was used by Melenka *et al* to compare nominal and printed sample dimensions [2].

Table 6: Comparison of MarkForged MarkOne sample width with nominal dimensions

Sample Measurement	Width Narrow (WN)			
	Nominal Dimension (mm)	13.00	% Difference	p -value
Sample 2R - Average (Standard Deviation)	13.09 (0.10)		0.72	<0.001
Sample 4R - Average (Standard Deviation)	13.11 (0.11)		0.86	<0.001
Sample 5R - Average (Standard Deviation)	13.09 (0.08)		0.72	<0.001
Sample Ny - Average (Standard Deviation)	13.05 (0.06)		0.39	<0.001

Table 7: Comparison of MarkForged MarkOne sample end tab width with nominal dimension

Sample Measurement		Width End Tab 1 (W1)		
Nominal Dimension (mm)		19.00	% Difference	<i>p</i> -value
Sample 2R - Average (Standard Deviation)		19.06 (0.06)	0.46	<0.001
Sample 4R - Average (Standard Deviation)		19.14 (0.08)	1.15	<0.001
Sample 5R - Average (Standard Deviation)		19.10 (0.08)	0.81	<0.001
Sample Ny - Average (Standard Deviation)		19.06 (0.17)	0.46	0.015

Table 8: Comparison of MarkForged MarkOne sample end tab width with nominal dimension

Sample Measurement		Width End Tab 2 (W2)		
Nominal Dimension (mm)		19.00	% Difference	<i>p</i> -value
Sample 2R - average (standard deviation)		19.08 (0.071)	0.66	<0.001
Sample 4R - average (standard deviation)		19.13 (0.09)	1.02	<0.001
Sample 5R - average (standard deviation)		19.09 (0.09)	0.71	<0.001
Sample Ny - average (Standard Deviation)		19.037 (0.06)	0.29	<0.001

Table 9: Comparison of MarkForged MarkOne sample thickness with nominal dimension

Sample Measurement		Thickness (T)		
Nominal Dimension (mm)		3.20	% Difference	<i>p</i> -value
Sample 2R - Average (Standard Deviation)		3.30 (0.03)	3.15	<0.001
Sample 4R - Average (Standard Deviation)		3.28 (0.03)	2.76	<0.001
Sample 5R - Average (Standard Deviation)		3.32 (0.07)	3.81	<0.001
Sample Ny - Average (Standard Deviation)		3.28 (0.02)	2.71	<0.001

3.2 *Microstructure Analysis*

The microstructure of the 3D printed samples was examined using a camera equipped with an optical microscope. Below, Figure 7 shows a sampling of the images obtained via optical microscopy. The first, Figure 7 (a), reveals the cross section of the fiber reinforced part. Here the shell, infill, and Kevlar regions can be clearly identified. In the Kevlar regions, nylon gaps can be observed between each of the concentric rings of reinforcing fiber. Figure 7 (b) highlights the waviness of the reinforcing fibers. The mechanical significance and potential impact of this misalignment will be further discussed in Section 4.3. Figure 7 (c) shows the fiber path at the corner of the printed part. Note that this particular sample was not ground parallel to the sample, and thus some of the fiber reinforcement appears to have been removed. Figure 7 (d) was not mounted in epoxy resin and is an image of the failure location. This image supports the proposition that fiber pull-out may have been a primary failure mechanism for the failure of the part, as will be discussed in Section 4.4. Note a large portion of the matrix has been displaced independent of the fibers, indicating insufficient adhesion between the fibers and matrix.

3.3 Mechanical Testing Results

Mechanical testing was performed on four sample configurations (Ny, 2R, 4R and 5R) to examine the effect of fiber reinforcement on the mechanical properties. The resulting stress-strain diagrams for the four sample configurations are shown in Figure 8. The stress-strain curves shown in Figure 8 demonstrate the effect of variations to the Kevlar reinforcement of the 3D printed samples on stress-strain behavior.

The elastic modulus of each sample configuration was determined from the stress-strain curves shown in Figure 8. The average elastic moduli for the four sample configurations are shown in Figure 9. This figure shows the resulting elastic moduli and standard deviation for each sample configuration. Figure 9 demonstrates that an increase in fiber reinforcement results in an increase in elastic modulus. This figure also shows that fiber reinforcement results in a dramatic increase in elastic modulus compared to Nylon only 3D printed samples.

The ultimate tensile strength of the fiber reinforced test samples was also examined. Figure 10 shows the resulting average ultimate tensile strength and standard deviation for the three fiber-reinforced sample configurations. This figure demonstrates that as fiber reinforcement increases, the ultimate tensile strength of the fiber reinforced 3D printed components also increases. The Nylon only samples were excluded from this comparison as failure was not achieved during testing due to their high toughness.

3.4 Elastic Constant Prediction for Fiber Reinforced 3D Printed Parts

The effective elastic constants of the fiber reinforced 3D printed samples were predicted using a rule of mixtures and volume average stiffness mathematical model described in Section 2.3. The geometric values shown in Table 5 were used to estimate the contribution of the Solid, infill, and fiber sections of the test specimen. The mechanical properties of the Nylon filament and Kevlar fibers were assumed based on the values in Table 3 and Table 4.

The resulting predicted elastic moduli for the four sample configurations investigated are shown in Figure 11. Figure 11 demonstrates that the VAS model predicts and increase in elastic modulus as fiber reinforcement increases.

4 Discussion

4.1 Dimensional Measurement

The dimensional accuracy of the MarkOne 3D printer was evaluated. The dimensions of the 3D printed test specimen were compared with nominal CAD dimensions for the 3D printed geometry. Tables 6 to 9 demonstrate that the printed sample geometries differed from the nominal CAD part dimensions. The results in Table 6 through 9 are consistent with other studies that have evaluated the dimensional accuracy of desktop 3D printed parts [2]. Table 6 to Table 9 show that the measure sample dimensions typically vary ± 0.1 mm from the nominal dimensions of the original CAD model. Understanding the dimensional accuracy of desktop 3D printers is necessary as this allows designers to select appropriate fits and tolerances for functional components produced using this manufacturing method. A comprehensive understanding of geometric accuracy can aid the designer in predicting error and compensating for the inherent limitations of the 3D printer.

4.2 Microstructure Analysis

The images produced from the optical microscopy analysis are of sufficient quality for qualitative analysis. Some error was noted in the alignment of specimen plane to the ground sample plane, as can be easily seen in Figure 7 (c). This is a result of the manual polishing approach that was used. As well, it was noted that debris collected in the larger voids of the sample (most notably in the infill regions), contributing to the scratches that can be seen in the images. Additionally, a lack of wetting of Kevlar fibers in the printed sample led to some fraying of fibers during the grinding and polishing, degrading the quality of the polished surface as this would lead to fiber debris during the final polishing steps.

4.3 Mechanical Testing

The stress-strain plots in Figure 8 demonstrate the effect of fiber reinforcement on the behavior of fiber reinforced 3D printed components. The stiffness, ultimate strength and ultimate strain all increase as the quantity of fiber reinforcement increases. Figure 8 also demonstrates the increase in stiffness of fiber reinforced 3D printed components relative to Nylon only samples. This is expected because of the Kevlar fibers have a much greater elastic modulus and

ultimate tensile strength than Nylon. Therefore, the addition of Kevlar fibers results in an increase in the effective properties of the 3D printed samples.

The stress-strain curves in Figure 8 (b)-(d) demonstrate non-linear behavior. The non-linear behavior of the fiber-reinforced 3D printed specimen is due to the MarkOne 3D printer manufacturing process. Kevlar fibers are embedded into the test specimen in specific regions of the 3D printed part. During the fiber embedding process however tension is not applied to the Kevlar strands, as a result fiber waviness occurs in the Kevlar strands (shown in Figure 12). This figure shows that the Kevlar fibers are not completely aligned with the longitudinal axis of the test sample. Fiber waviness affects the mechanical properties of the 3D printed parts as the embedded fibers are not entirely aligned with the loading axis of the test samples. The effect of fiber waviness on the mechanical properties of composite laminates was demonstrated by Hsiao *et al* [22]. As the samples are loaded the embedded fibers begin to straighten due to the applied tensile load. This straightening of the embedded yarns explains the non-linear behavior of the samples shown in Figure 8 (b)-(d).

The effect of fiber reinforcement on 3D printed parts is shown in Figure 9 and Figure 10. **Error! Reference source not found.** These figures demonstrate that both the elastic modulus and ultimate tensile strength increase as fiber reinforcement increases.

The failure location for the fiber reinforced 3D printed samples was consistent for all samples tested. The failure location can be seen in Figure 13. In this figure, the fiber placement path generated using the Eiger 3D printing software and a failed sample is shown. It can be seen that sample failure occurs at the location where the fiber path begins for the sample. All geometries manufactured using the MarkOne 3D printer will have a start location for the continuous fiber reinforcement. Figure 13 demonstrates that understanding the start location of the fiber reinforcement is critical for manufacturing functional components. When designing components to be manufactured using this 3D printing method the start location of the fiber reinforcement should be placed in a position of low loading in order to prevent premature failure due to the stress concentration caused by the fiber start location.

4.4 Comparison of mechanical model results with experiments

The mechanical properties of the fiber reinforced 3D printed specimen were predicted using a volume averaging stiffness method. This approach allows for the mechanical properties of the fiber reinforcement and thermoplastic filament to be taken into account. In addition, the volume averaging method allows for the contribution of the different internal structures of the fiber reinforced 3D printed components to be analyzed.

The results from experimental analysis of the fiber reinforced 3D printed specimen and the predicted elastic modulus for the test specimen are compared in Table 10. This table shows good agreement between the predicted elastic modulus for the fiber reinforced 3D printed test samples with the experimental test data. In particular, the 4 and 5 concentric Kevlar ring samples differed from experiment by 6.2 and 0.1% respectively. A larger discrepancy was determined for the 2 concentric ring fiber reinforced samples. In this case the predicted and experimental results differed by 57.5%. This difference could again be due to the waviness of the Kevlar fibers. The lower experimental modulus could be due to the misalignment of the Kevlar yarns with respect to the longitudinal axis. The misalignment of the fiber yarns will result in a reduction in the elastic modulus of the test samples. The volume averaging method assumes that the Kevlar yarns are straight and no waviness in the yarns exists. The large discrepancy between the volume averaging results and test results for the 2 concentric ring sample could also be due to the fiber volume fraction. The 2 concentric rings samples have a fiber volume fraction of 4.0%. The low fiber volume fraction could be below the lower limit which is valid for the volume average stiffness method. Another reason for the difference between the model results for the 2 concentric ring samples could also be due to poor bonding between the fibers and the nylon matrix. Composite material models assume that fibers and matrix are perfectly bonded [21]. Imperfect fiber-matrix bonds could result in fiber pull-out or slipping which would result in a lower elastic modulus than the predicted modulus. The results shown in Table 10 show that higher fiber volume fractions are better predicted using the volume averaging method, therefore the methodology presented in this manuscript should be used for modeling structures that have fiber volume fractions of 8% and above. As shown in this study greater fiber reinforcement results in an increase in stiffness and ultimate strength, therefore high volume fractions of fibers should be used for stiffness and strength critical applications. Additionally, different fiber reinforcement patterns may be useful to improve the mechanical

properties of fiber reinforced 3D printed parts. This study examined concentric fiber reinforcement but the Eiger 3D printing software also allows for full layers of fiber reinforcement.

Table 10: Comparison of measured and predicted elastic modulus for fiber reinforced 3D printed test samples

	2 Concentric Rings Average (StDev)	4 Concentric Rings Average (StDev)	5 Concentric Rings Average (StDev)
Elastic Modulus			
Experimental (MPa)	1767.2 (39.3)	6920.0 (272.3)	9001.2 (314.2)
Elastic Modulus Predicted (Mpa)	4155.7	7380.0	8992.1
% Difference	57.5	6.2	0.1
Fiber Volume Fraction (Vf) %	4.04	8.08	10.1

The comparison in Table 10 demonstrates that the volume averaging method can be used to effectively predict the mechanical properties of fiber reinforced 3D printed parts with higher number of fiber rings. The volume averaging method described in Section 2.3 has been implemented so that designers can quickly predict the mechanical properties of fiber reinforced 3D printed components. The approach described in this section can be used to predict the mechanical properties of other fiber reinforcing materials including Glass Fiber and Carbon Fiber. Both of these fiber reinforcements are available for the MarkOne 3D printer.

5 Conclusions

The tensile properties of fiber reinforced 3D printed components were evaluated in this study. Tensile tests were performed on four combinations of samples that were produced using the MarkOne 3D printer. The testing results demonstrated that an increase in the volume of fiber reinforcement results in an increase in stiffness and ultimate strength of the test samples.

In addition, a volume averaging stiffness method has been developed in order to predict the tensile properties of the fiber reinforced 3D printed samples. The experimental and predictive model results demonstrated good agreement in particular for sample configurations with higher fiber volume fractions. The predictive model allows for the tensile properties of fiber reinforced 3D printed parts, in particular for sample configurations with higher fiber volume fractions, to be easily predicted. This model will allow for designers to predict the tensile properties of fiber reinforced 3D printed parts so that they can be used for functional applications which require specific tensile properties. This study provides a basis for predicting the tensile properties of fiber reinforced 3D printed structure. Further research is required to fully characterize the mechanical behavior of these structures. Compression, bending and torsion tests are required in order to fully characterize the mechanical behavior of these fiber reinforced 3D printed structures.

Acknowledgements

The authors would like to thank Bernie Falkner for his assistance with the mechanical testing of the test specimen. We would also like to thank Patrick Pilarski for allowing for us to use his 3D printer for this study.

6 List of Figures

Figure 1: Test specimen geometry for tensile testing of 3D printed parts. Geometry specified according to ASTM D638-14

Figure 2: Concentric ring reinforcement of test specimens. 5R-five concentric Kevlar fiber rings. 4R- four concentric Kevlar rings. 2R- two concentric Kevlar rings. 0R- no Kevlar reinforcement

Figure 3: Mechanical testing setup to evaluate the tensile properties of Kevlar reinforced 3D printed specimen

Figure 4: Schematic of the structure of the fiber reinforced 3D printed test specimen. Left: top view of the 3D printed test specimen. Right: Cross-sectional view (Section A-A) of the test specimen. Solid regions are represented as solid white rectangles, infill regions have a hatch pattern and Kevlar reinforced regions are represented as yellow.

Figure 5: Cross-sectional image of a test specimen. The shell, infill and Kevlar regions of the test specimen are shown

Figure 6: Top view of a test sample showing the orientation of the solid layers. Solid layers are oriented 45° from the longitudinal axis

Figure 7: Microscope images of fiber reinforced 3D printed parts, showing (a) cross section with shell, Kevlar, and infill regions; (b) waviness of reinforcing fibers; (c) close-up of fiber orientation at corner; and (d) fiber pull-out consistent with failure locations.

Figure 8: Stress-strain curves for the four Kevlar fiber reinforcement configurations (a) Nylon only sample configuration (b) Two-concentric Kevlar rings configuration (c) Four concentric Kevlar rings configuration (d) Five concentric Kevlar rings configuration

Figure 9: Comparison of the experimentally determined elastic moduli of the four fiber reinforced 3D printed sample configurations

Figure 10: Comparison of experimentally measured fiber reinforced 3D printed test samples ultimate strength

Figure 11: Predicted elastic moduli for fiber reinforced 3D printed samples using a volume averaging stiffness method

Figure 12: Cross-sectional view of a Kevlar reinforced 3D printed test sample. The waviness of Kevlar fibers demonstrated in this image.

Figure 13: Sample failure location. Sample failure occurs at the starting location of the Kevlar fiber reinforcement

7 References

- [1] I. Gibson, D. Rosen and B. Stucker, *Additive Manufacturing Technologies : 3D Printing, Rapid Prototyping, and Direct Digital Manufacturing*. New York, NY : Springer, 2015; Second edition, 2015.
- [2] G. W. Melenka, J. S. Schofield, M. R. Dawson and J. P. Carey, "Evaluation of dimensional accuracy and material properties of the MakerBot 3D desktop printer," *Rapid Prototyping Journal*, vol. 21, pp. 618-627, 2015.
- [3] J. F. Rodriguez, J. P. Thomas and J. E. Renaud, "Characterization of the mesostructure of fused-deposition acrylonitrile-butadiene-styrene materials," *Rapid Prototyping Journal*, vol. 6, pp. 175-186, 2000.
- [4] S. Ahn, M. Montero, D. Odell, S. Roundy and P. K. Wright, "Anisotropic material properties of fused deposition modeling ABS," *Rapid Prototyping Journal*, vol. 8, pp. 248-257, 2002.
- [5] J. F. Rodríguez, J. P. Thomas and J. E. Renaud, "Mechanical behavior of acrylonitrile butadiene styrene fused deposition materials modeling," *Rapid Prototyping Journal*, vol. 9, pp. 219-230, 2003.
- [6] ColorFab. *ColorFab BrassFill 3D Printing Filament*. Available: <http://colorfabb.com/brassfill>. 2016
- [7] 3DXTech, "Carbon Fiber Reinforced PLA Filament," 2014.
- [8] K. Mori, T. Maeno and Y. Nakagawa, "Dieless Forming of Carbon Fibre Reinforced Plastic Parts Using 3D Printer," *Procedia Engineering*, vol. 81, pp. 1595-1600, 2014.

- [9] A. Kreger and G. Teters, "Use of averaging methods to determine the viscoelastic properties of spatially reinforced composites," *Mechanics of Composite Materials*, vol. 15, pp. 377-383, 1980.
- [10] A. Kregers and Y. G. Melbardis, "Determination of the deformability of three-dimensionally reinforced composites by the stiffness averaging method," *Mechanics of Composite Materials*, vol. 14, pp. 1-5, 1978.
- [11] A. Kregers and G. Teters, "Determination of the elastoplastic properties of spatially reinforced composites by the averaging method," *Mechanics of Composite Materials*, vol. 17, pp. 25-31, 1981.
- [12] A. Kregers and A. Zilauts, "Limiting values of reinforcement factors for fibrous composites with a three-dimensional structure," *Mechanics of Composite Materials*, vol. 20, pp. 530-536, 1985.
- [13] ASTM D638-14, "Standard Test Method for Tensile Properties of Plastics," 2014.
- [14] J. Carey, M. Munro and A. Fahim, "Longitudinal elastic modulus prediction of a 2-D braided fiber composite," *J Reinf Plast Compos*, vol. 22, pp. 813-831, 2003.
- [15] C. Ayranci and J. P. Carey, "Predicting the longitudinal elastic modulus of braided tubular composites using a curved unit-cell geometry," *Composites Part B: Engineering*, vol. 41, pp. 229-235, 2010.
- [16] C. K. Leung, G. W. Melenka, D. S. Nobes and J. P. Carey, "The effect on elastic modulus of rigid-matrix tubular composite braid radius and braid angle change under tensile loading," *Composite Structures*, vol. 100, pp. 135-143, 2013.
- [17] G. W. Melenka, S. Hoxha, D. S. Nobes and J. P. Carey, "Analytical and experimental analysis of tubular braided composites," in *CANCOM 2015- Canadian International Conference on Composite Materials*, Edmonton, Alberta, Canada, 2015, .

[18] S. Kawabata, "Measurement of the transverse mechanical properties of high-performance fibres," *Journal of the Textile Institute*, vol. 81, pp. 432-447, 1990.

[19] MATWEB *Overview of materials for Nylon 6, Extruded*. Available: <http://www.matweb.com>, 2015

[20] I. M. Daniel and O. Ishai, *Engineering Mechanics of Composite Materials*. New York: Oxford University Press, 2006.

[21] R. M. Jones, *Mechanics of Composite Materials*. Washington, Scripta Book Co. 1975], 1975.

[22] H. Hsiao and I. Daniel, "Effect of fiber waviness on stiffness and strength reduction of unidirectional composites under compressive loading," *Composites Sci. Technol.*, vol. 56, pp. 581-593, 1996.

List of Figures

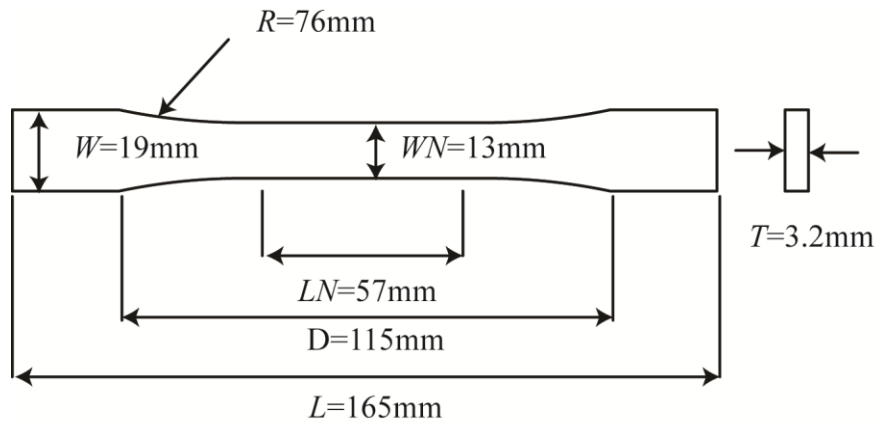


Figure 1: Test specimen geometry for tensile testing of 3D printed parts. Geometry specified according to ASTM D638-14

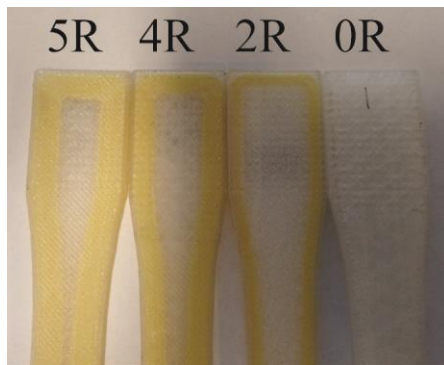


Figure 2: Concentric ring reinforcement of test specimens. 5R-five concentric Kevlar fiber rings. 4R- four concentric Kevlar rings. 2R- two concentric Kevlar rings. 0R- no Kevlar reinforcement

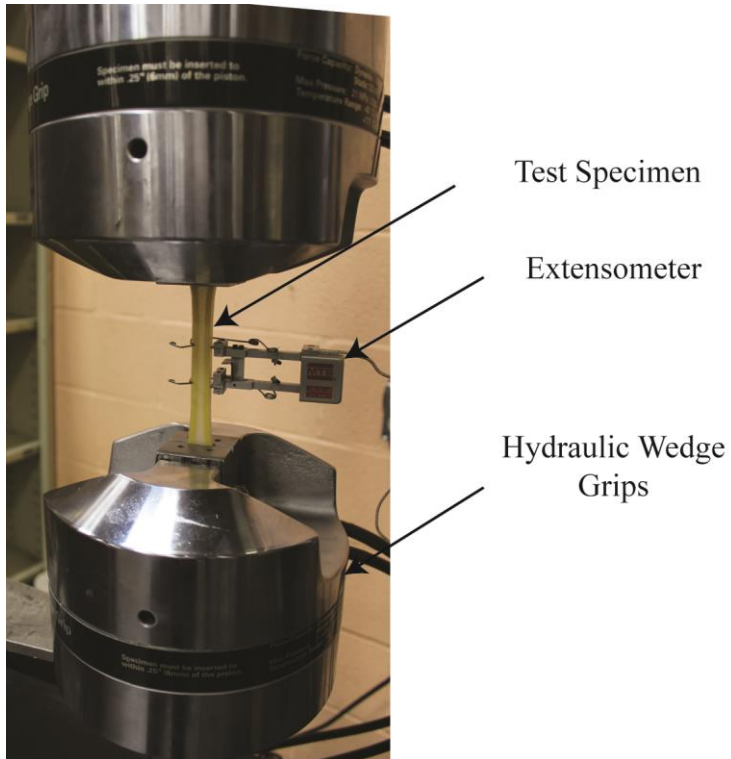


Figure 3: Mechanical testing setup to evaluate the tensile properties of Kevlar reinforced 3D printed specimen

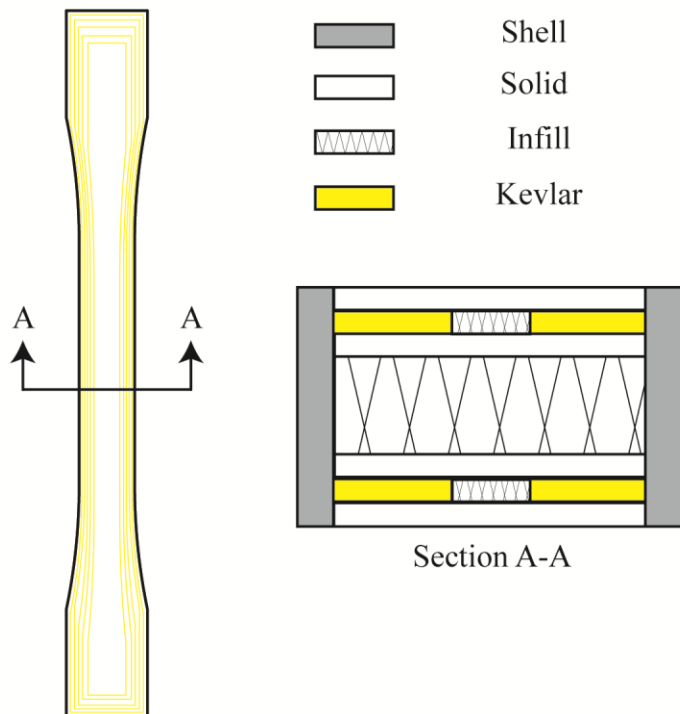


Figure 4: Schematic of the structure of the fiber reinforced 3D printed test specimen. Left: top view of the 3D printed test specimen. Right: Cross-sectional view (Section A-A) of the test specimen. Solid regions are represented as solid white rectangles, infill regions have a hatch pattern and Kevlar reinforced regions are represented as yellow.

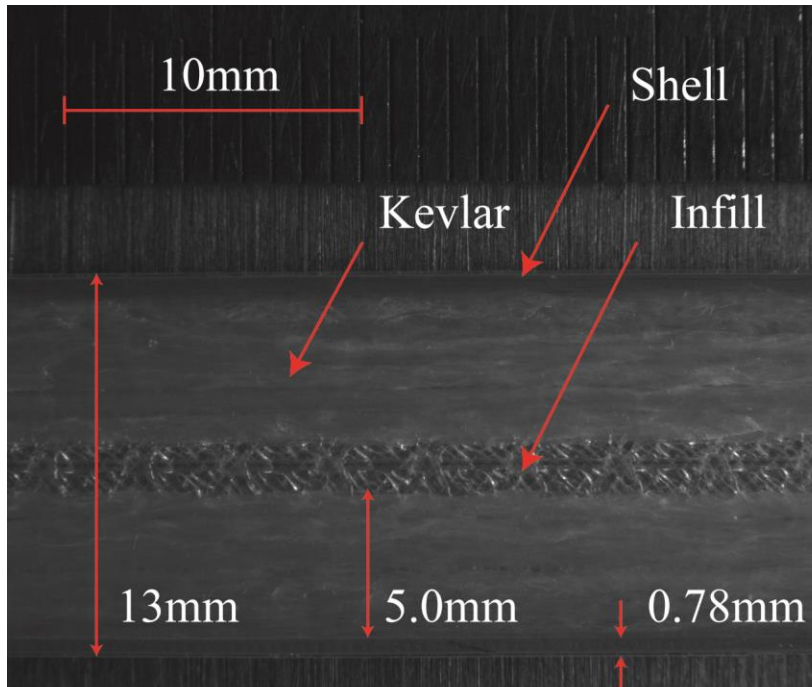


Figure 5: Cross-sectional image of a test specimen. The shell, infill and Kevlar regions of the test specimen are shown

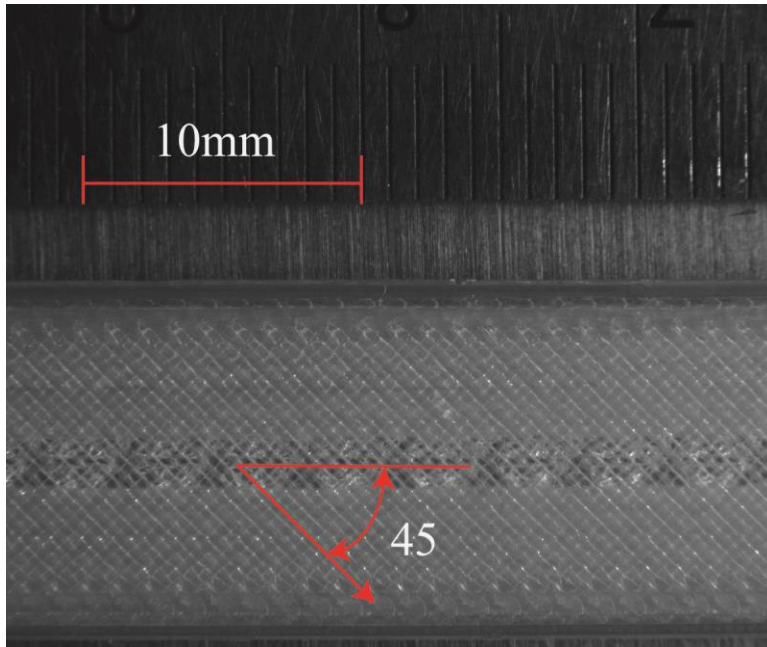


Figure 6: Top view of a test sample showing the orientation of the solid layers. Solid layers are oriented 45° from the longitudinal axis

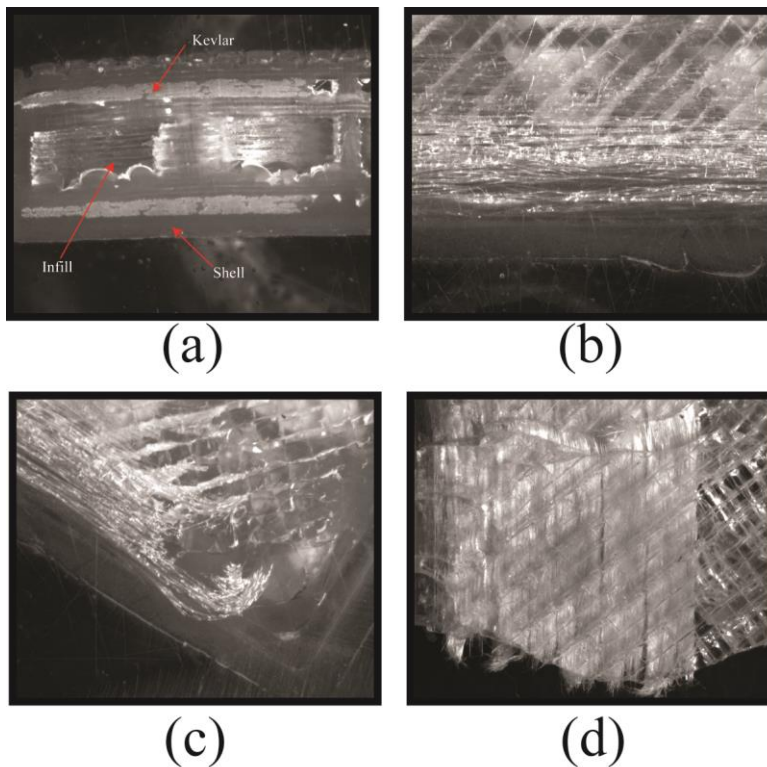
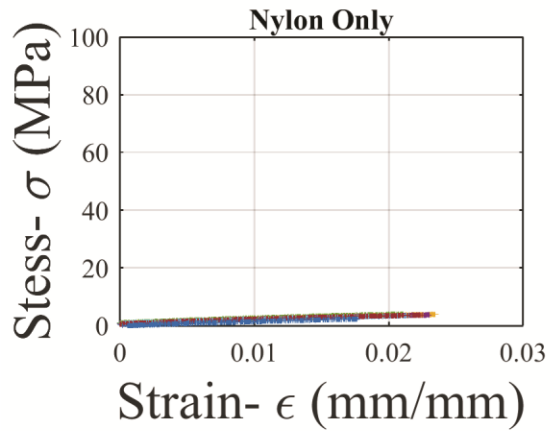
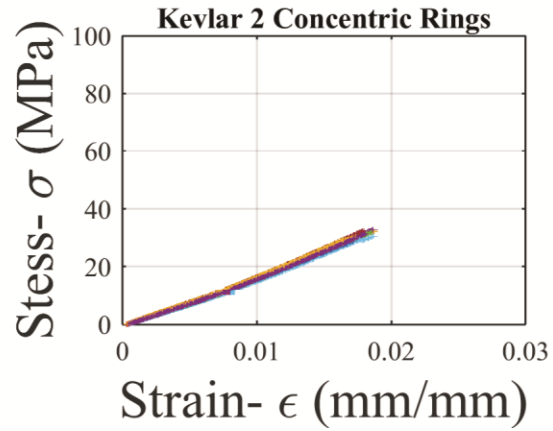


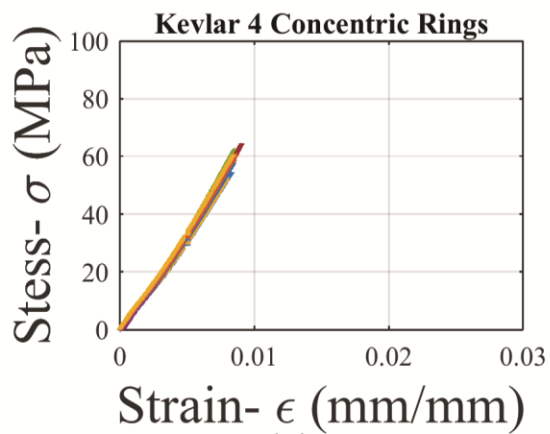
Figure 7: Microscope images of fiber reinforced 3D printed parts, showing (a) cross section with shell, Kevlar, and infill regions; (b) waviness of reinforcing fibers; (c) close-up of fiber orientation at corner; and (d) fiber pull-out consistent with failure locations.



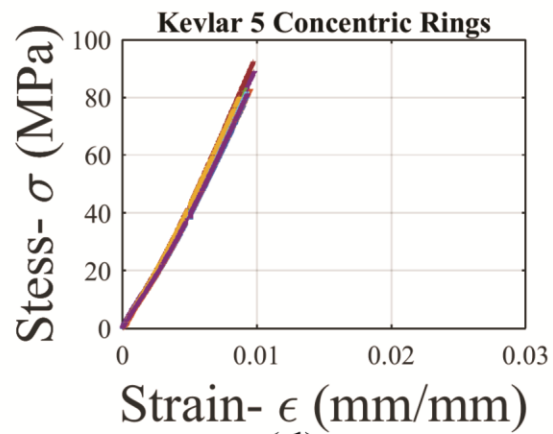
(a)



(b)



(c)



(d)

Figure 8: Stress-strain curves for the four Kevlar fiber reinforcement configurations (a) Nylon only sample configuration (b) Two-concentric Kevlar rings configuration (c) Four concentric Kevlar rings configuration (d) Five concentric Kevlar rings configuration

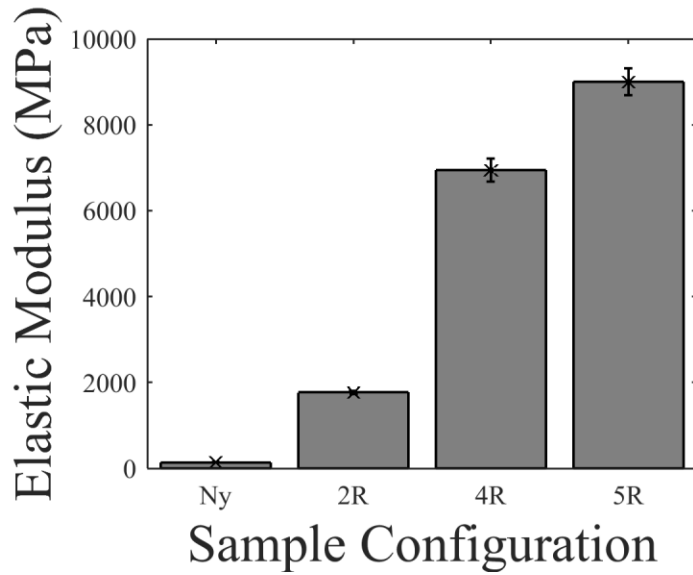


Figure 9: Comparison of the experimentally determined elastic moduli of the four fiber reinforced 3D printed sample configurations

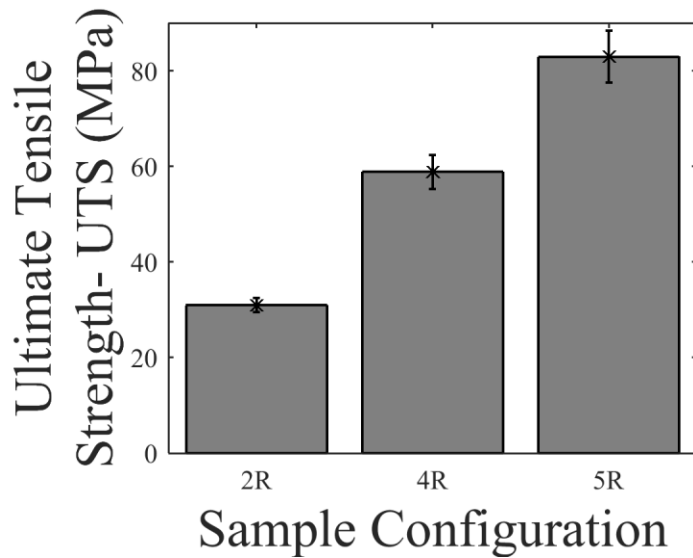


Figure 10: Comparison of experimentally measured fiber reinforced 3D printed test samples ultimate strength

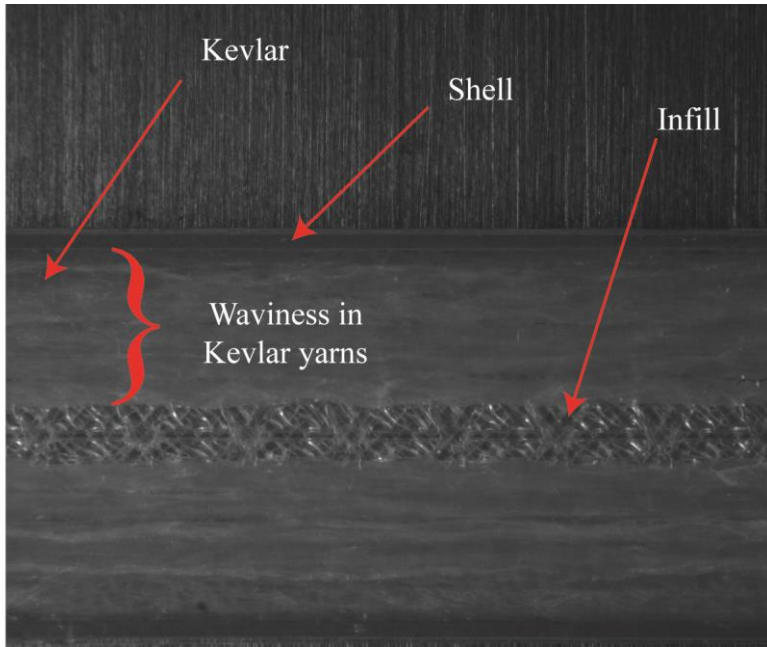


Figure 11: Predicted elastic moduli for fiber reinforced 3D printed samples using a volume averaging stiffness method

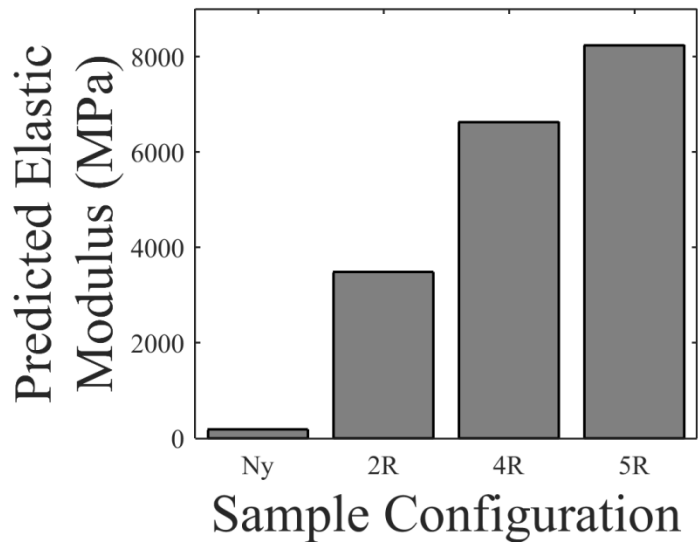


Figure 12: Cross-sectional view of a Kevlar reinforced 3D printed test sample. The waviness of Kevlar fibers demonstrated in this image.

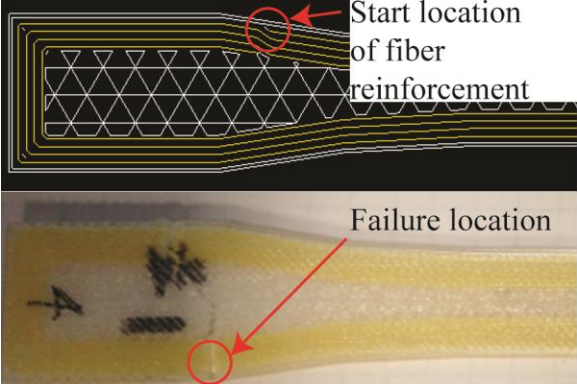


Figure 13: Sample failure location. Sample failure occurs at the starting location of the Kevlar fiber reinforcement